Supporting Information

Sodium Alginate-Based Coaxial Fibers Synergistically Integrate Moisture Actuation, Length Tracing, Humidity Sensing, and Electric Heating

Lizhong Dong,[a] Ming Ren,[a] Yulian Wang,[a] Xiaojie Yuan,[a] Xiaobo Wang,[ab] Guang Yang,[ab] Yuxin Li,[ab] Wei Li,[a] Yunfeng Shao,[ab] Guanlong Qiao,[a] Weiwei Li,[a] Hongli Sun,[a] Jiangtao Di,*[ab] Qingwen Li[ab]

[a]Advanced Materials Division, Key Laboratory of Multifunctional Nanomaterials and Smart Systems, Suzhou Institute of Nano-Tech and Nano-Bionics, Chinese Academy of Sciences, Suzhou 215123, China

[b]School of Nano-Technology and Nano-Bionics, University of Science and Technology of China, Hefei 230026, China

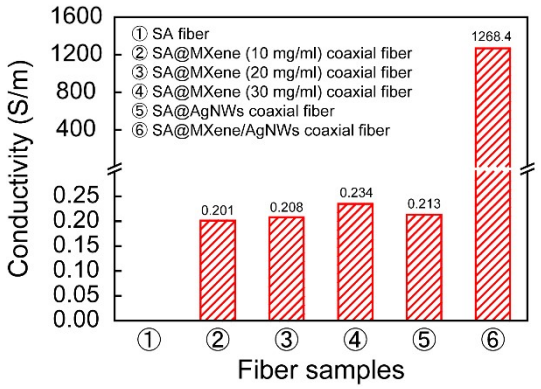

Fig. S1. Conductivity of different fiber samples.

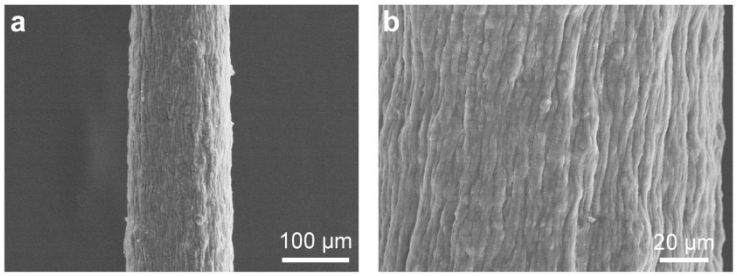

Fig. S2. SEM images of the SA fiber (159.82 μm in diameter).

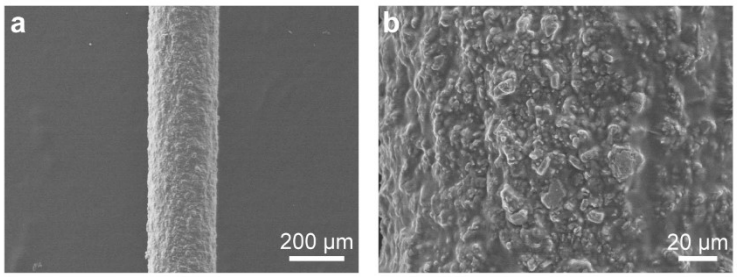

Fig. S3. SEM images of the SA@MXene coaxial fiber (264.42 μm in diameter).

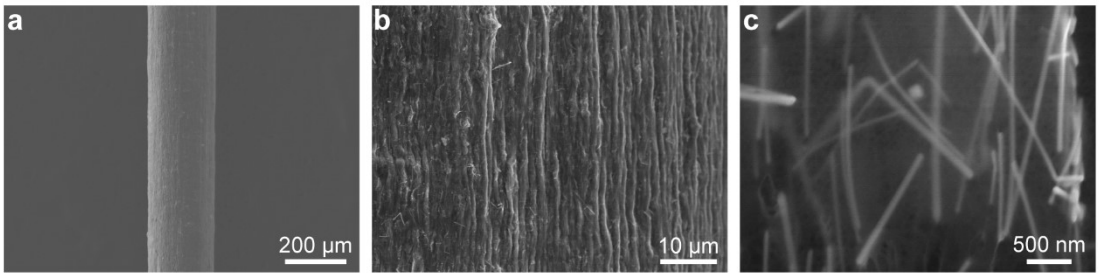

Fig. S4. SEM images of the SA@AgNWs coaxial fiber (248.88 μm in diameter).

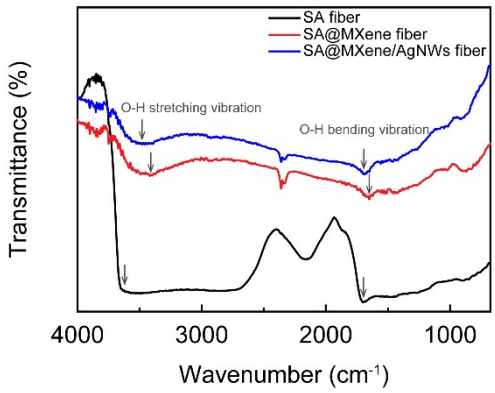

Fig. S5. FTIR spectra of the SA fiber, SA@MXene coaxial fiber, and SA@MXene/AgNWs coaxial fiber.

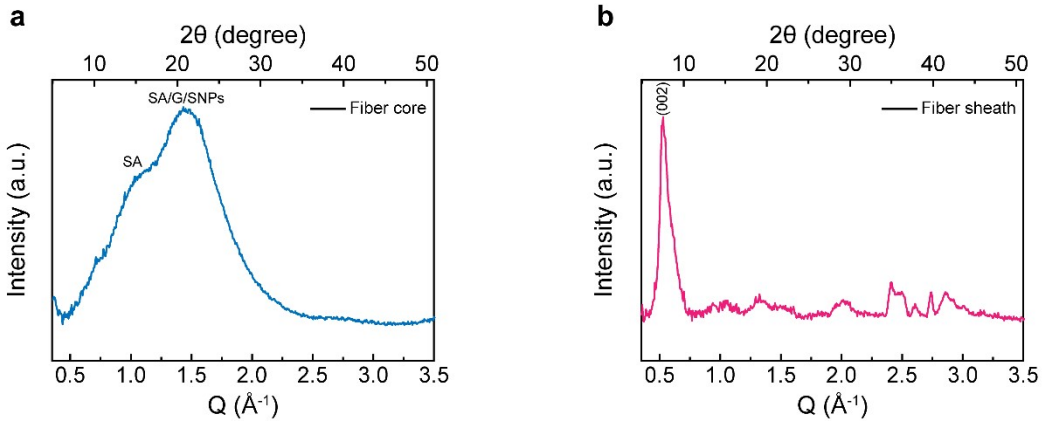

Fig. S6 WAXS patterns. (a) Fiber core. (b) Fiber sheath.

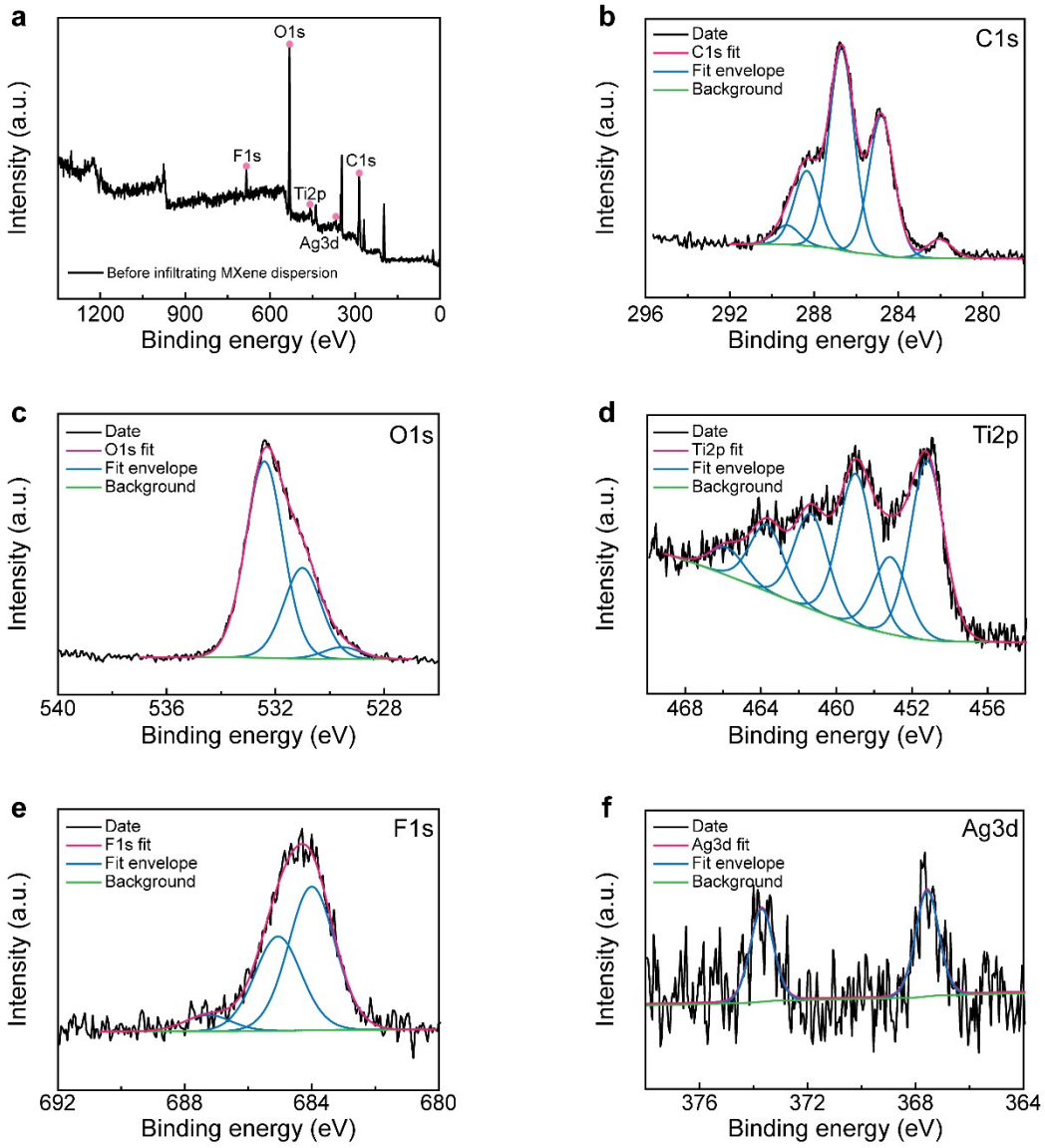

Fig. S7. XPS spectra of the coaxial fiber before infiltrating the MXene dispersion. (a) Full region. (b) C1s region. (c) O1s region. (d) Ti2p region. (e) F1s region. (f) Ag3d region.

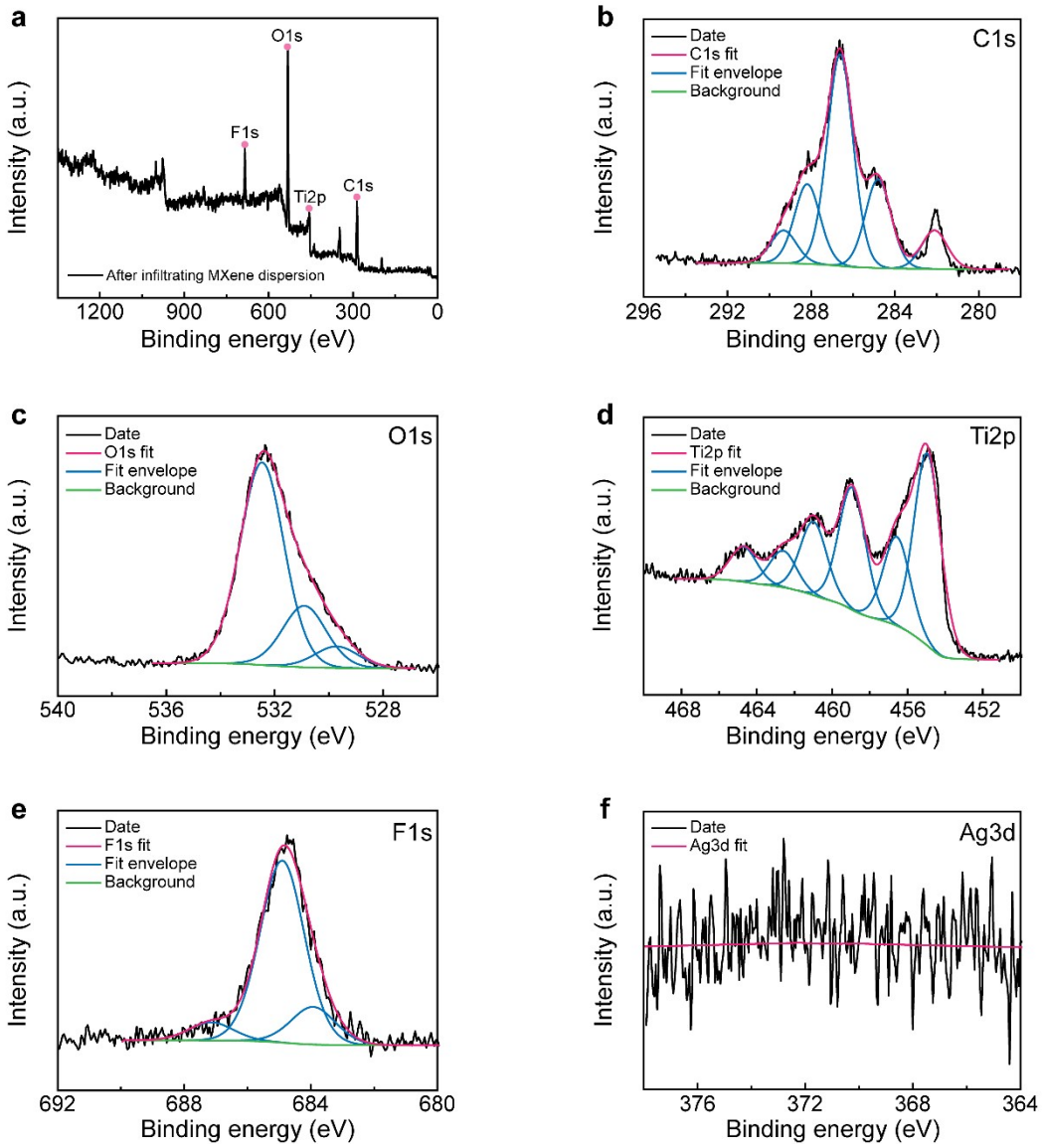

Fig. S8. XPS spectra of the coaxial fiber after infiltrating the MXene dispersion. (a) Full region. (b) C1s region. (c) O1s region. (d) Ti2p region. (e) F1s region. (f) Ag3d region.

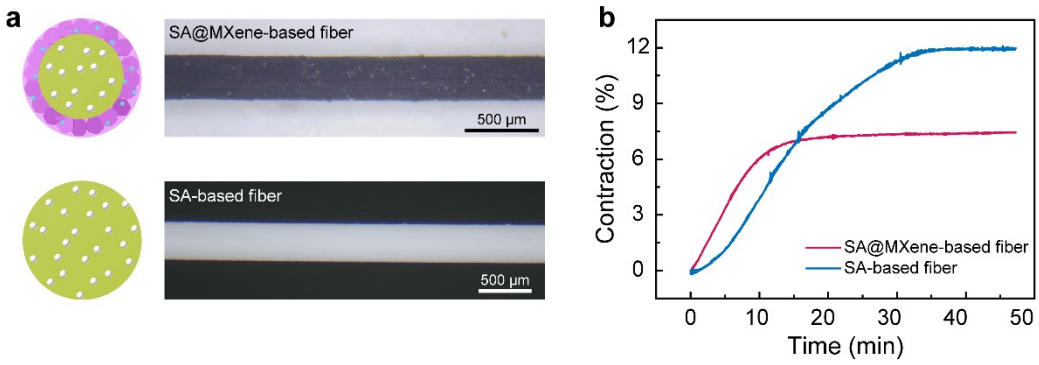

Fig. S9. Comparison of water molecule transport speed between the SA@MXene coaxial fiber and SA fiber with the same diameter in air environment.

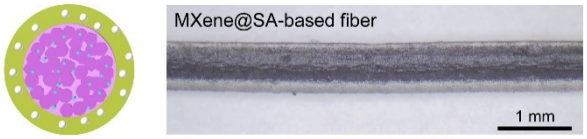

Fig. S10. Structure schematic illustration and optical photograph of the MXene@SA coaxial fiber.

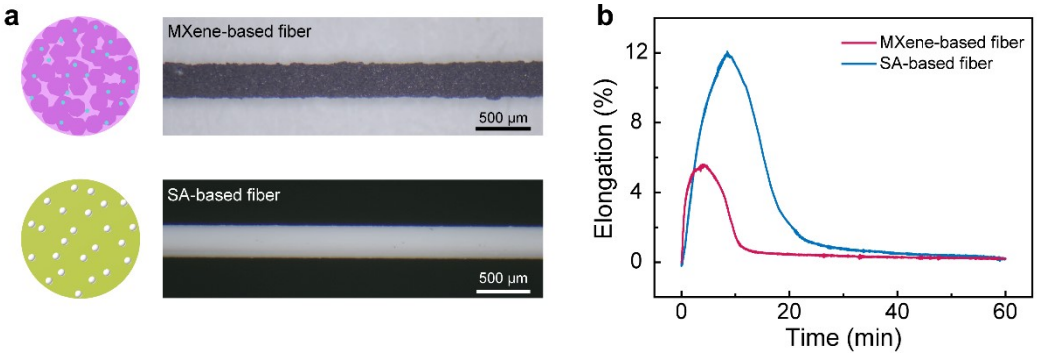

Fig. S11. Comparison of elongation between the MXene fiber and SA fiber with the same diameter after absorbing water molecules.

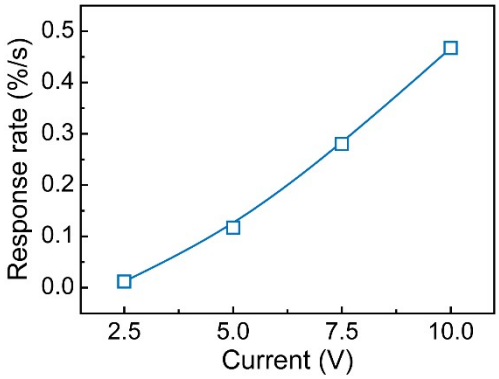

Fig. S12. The relationship between contraction response rate and different voltages.

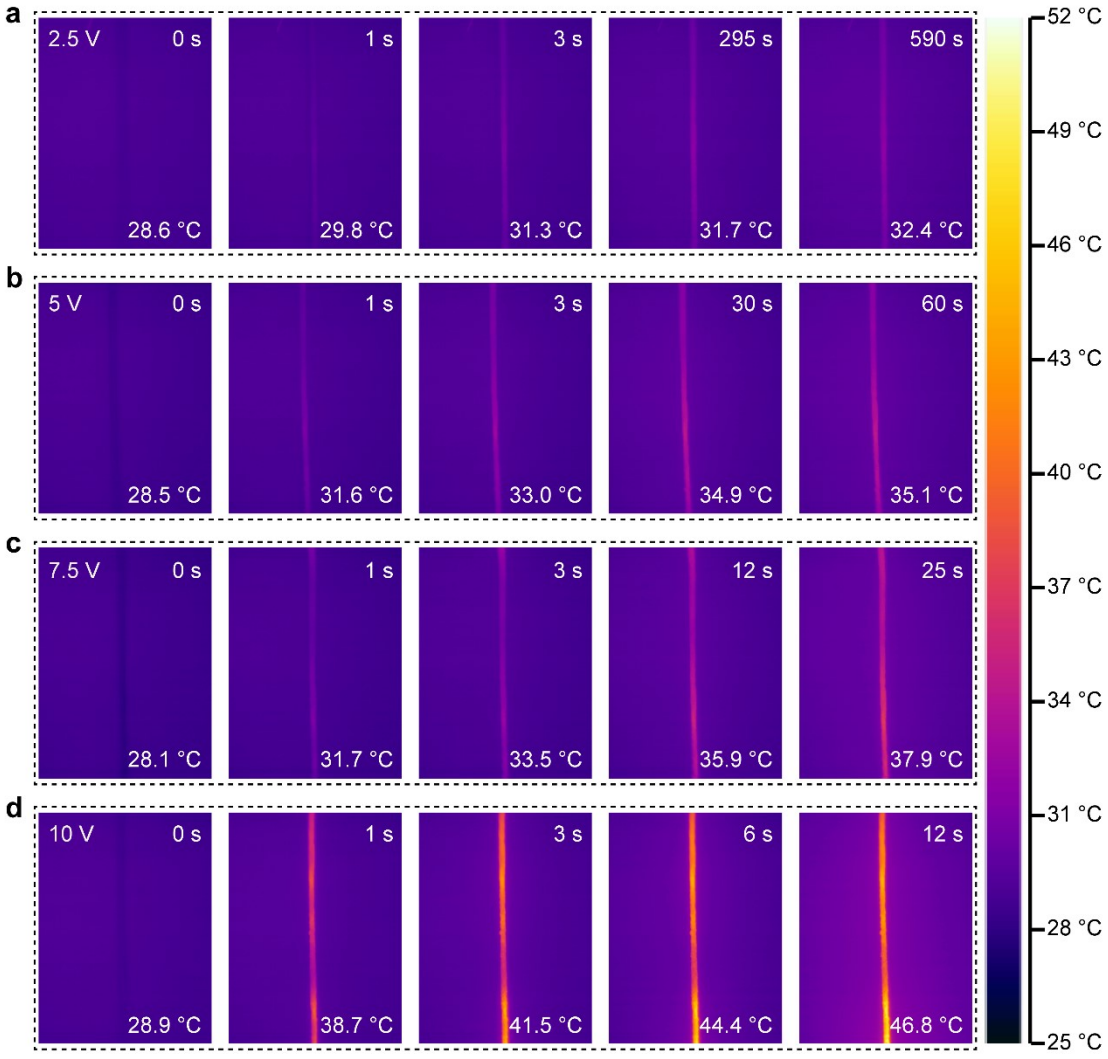

Fig. S13. The surface temperature of the coaxial fiber under different voltages during the contracted process. (a) 2.5 V; (b) 5 V; (c) 7.5 V; (d) 10 V.

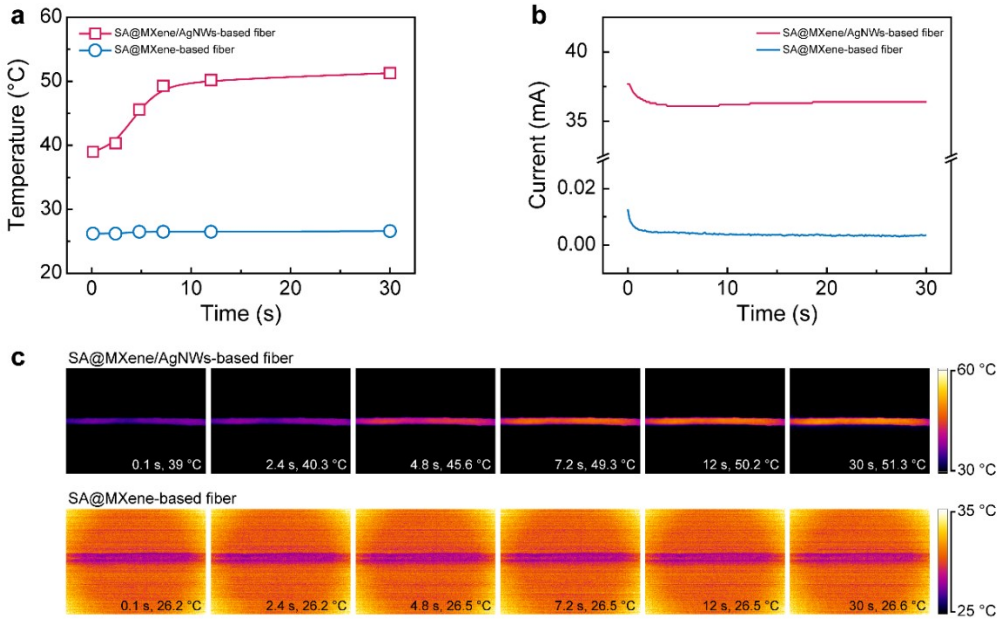

Fig. S14. The temperature and current changes of SA@NXene coaxial fibers before and after introducing AgNWs at 10 V voltage. (a) Temperature versus time of different coaxial fibers. (b) Current versus time of different coaxial fibers. (c) IR images at different times.

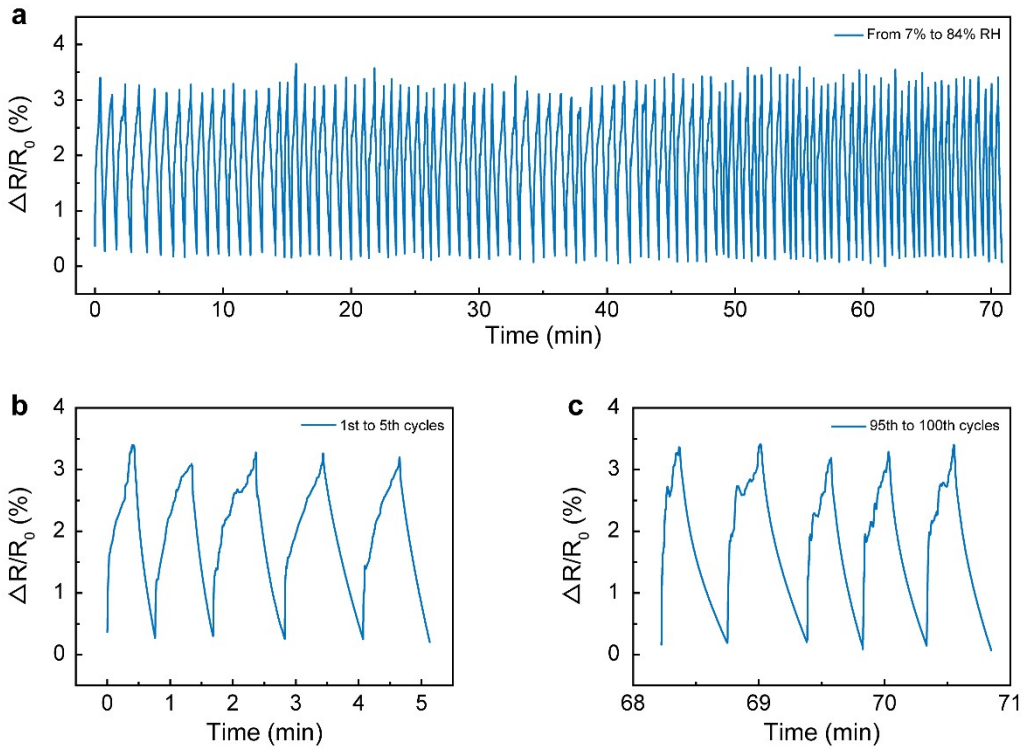

Fig. S15. 100 cycles of 7% and 84% RH environment switching test of the coaxial fiber.

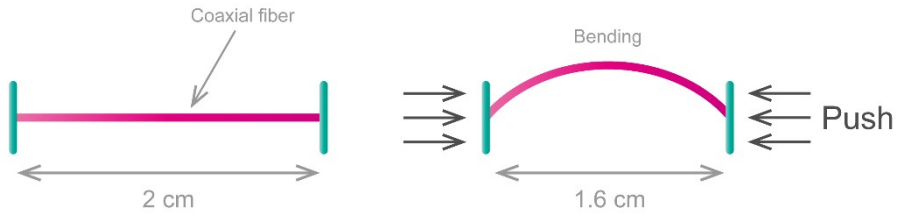

Fig. S16. Schematic illustration of the fiber bending test process, distance between the two ends of the pushing device from 2 cm to 1.6 cm.

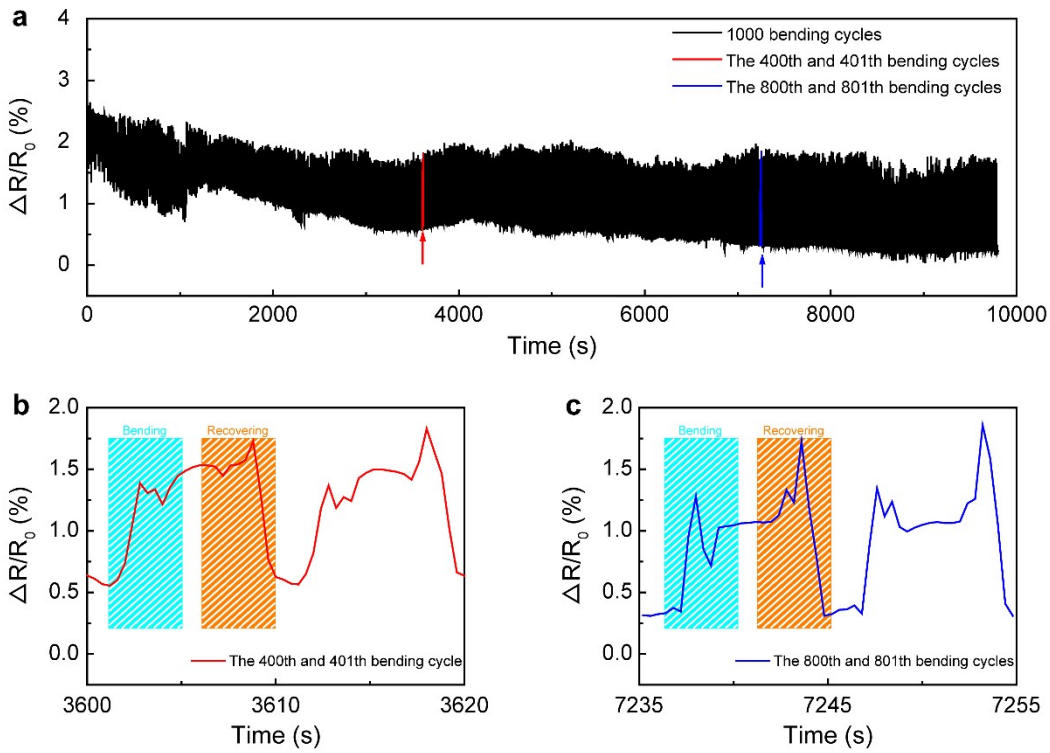

Fig. S17. Relative resistance change of the SA@MXene coaxial fiber during bending/recovery process. (a) Relative resistance change of the SA@MXene coaxial fiber during the 1000 bending cycles (the change of fiber length from 20 mm to 16 mm). (b) The relative resistance change during the 400th and 401th bending/recovery process. (c) The relative resistance change during the 800th and 801th bending/recovery process.

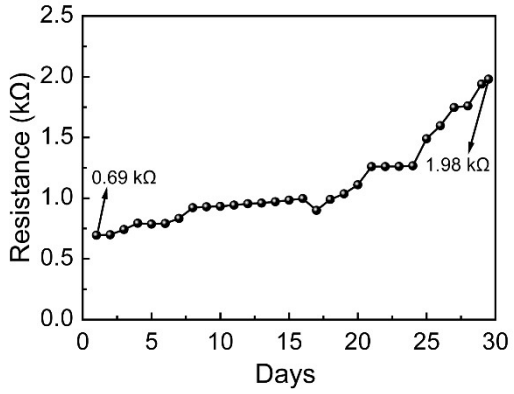

Fig. S18. The resistance change of the coaxial fiber (2-cm-long) exposed to the air for 30 days.

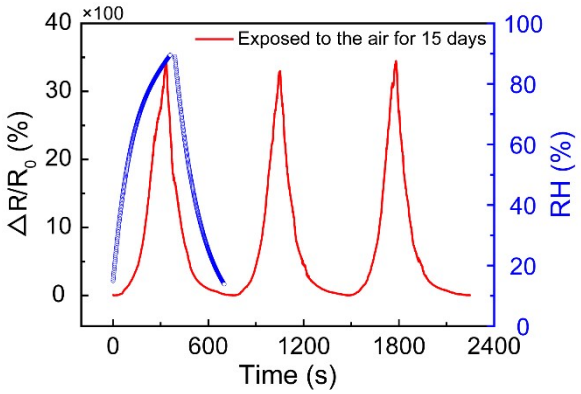

Fig. S19. Relative resistance change with RH of the SA@MXene coaxial fiber exposed to the air for 15 days.

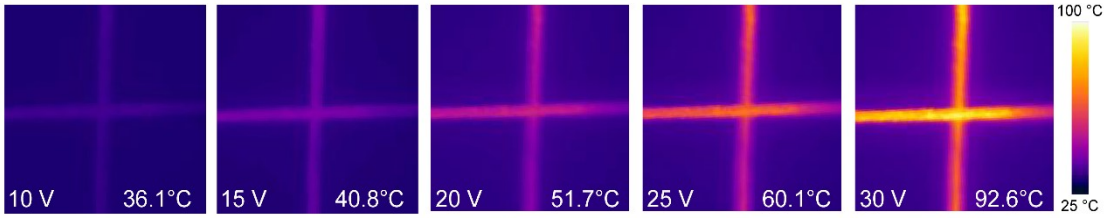

Fig. S20. FLIR images of the stable surface temperature of the thermal physiotherapy textile at different voltages (0 V, 10 V, 15 V, 20 V, 25 V, and 30 V).

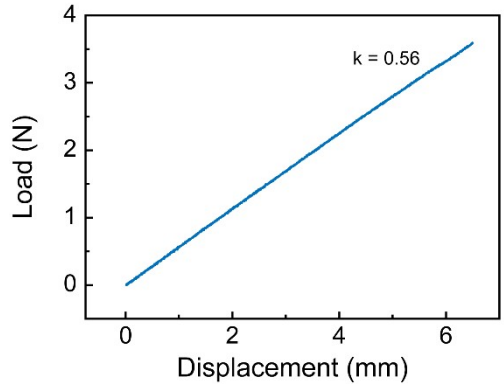

Fig. S21. Hooke coefficient of the spring used for the simultaneous testing of length and contractile force.

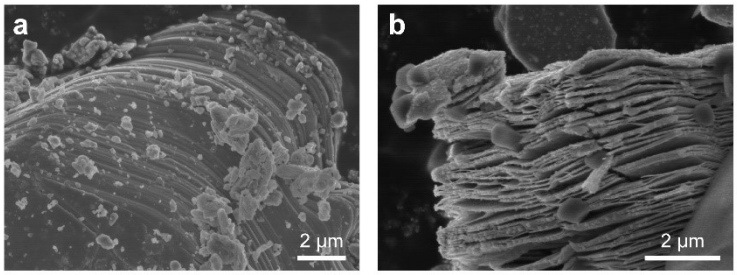

Fig. S22. Typical SEM images of the (a) Ti_3AlC_2 powder and (b) freeze-dried $Ti_3C_2T_x$ power.

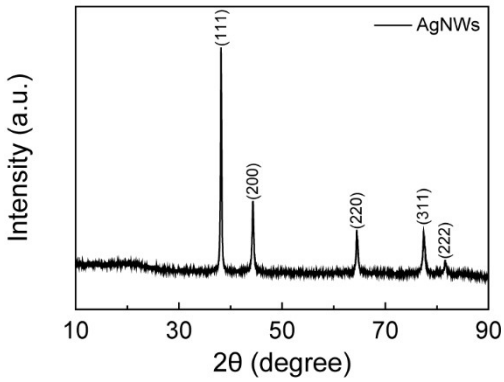

Fig. S23. XRD patterns of AgNWs.

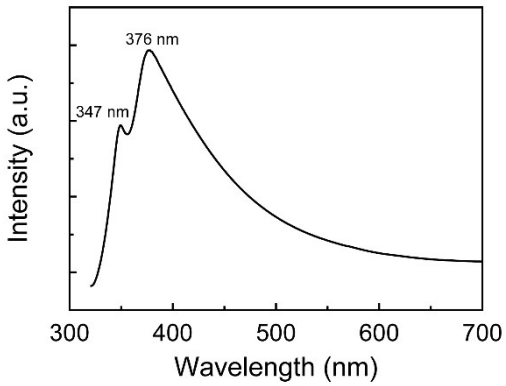

Fig. S24. UV-vis absorption spectra of water solution of AgNWs. The AgNWs exhibited a maximum absorption at about 376 nm with a shoulder peak at 347 nm prior to functionalization ($\Delta\lambda$ = 2 nm).

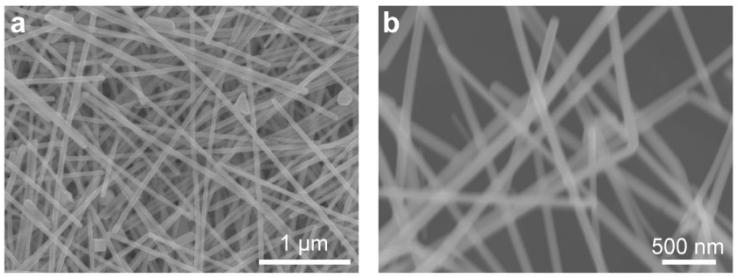

Fig. S25. SEM images of AgNWs.

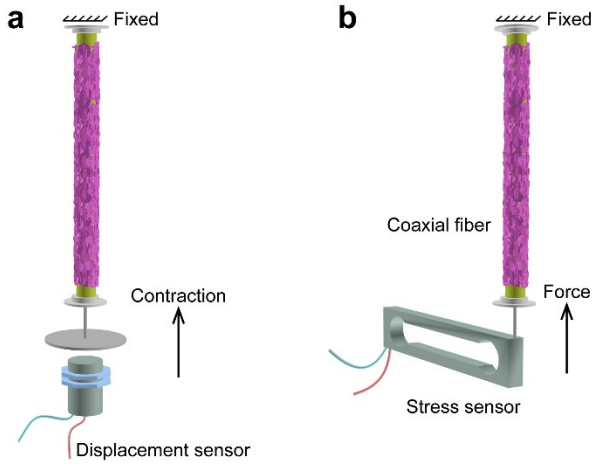

Fig. S26. Schematic diagram of the test equipments of (a) actuation stroke and (b) contractile force.

Table S1. Components of different fibers.

The inner core (22 G)			The outer sheath (17 G)		
SA (wt%)	G (wt%)	SNPs (wt%)	MXene (mg/ml)	AgNWs (mg/ml)	SA (wt%)
2.5	2.5	1	-	-	-
2.5	2.5	1	10	-	0.5
2.5	2.5	1	20	-	0.5
2.5	2.5	1	30	-	0.5
2.5	2.5	1	-	5	0.5
2.5	2.5	1	20	5	0.5

The calculation process of the conductivity of the coaxial fiber:

The resistivity calculation equation is as follows

$$\rho = RS/l \quad \text{(S1)}$$

where R, S, and l represent the resistance, cross-sectional area, and length of the coaxial fiber, respectively.

Since the inner core in the coaxial fiber has no electrical conductivity, the cross-sectional area was rewritten to the following formula

$$S = \pi r_2^2 - \pi r_1^2 \quad \text{(S2)}$$

where r_1 and r_2 represent the radius of the inner core fiber and the coaxial fiber, respectively.

The conductivity calculation equation is as follows

$$\sigma = 1/\rho \quad \text{(S3)}$$